Carbon Dioxide Absorption by Monoethanolamine in Hollow Fiber Membrane Contactors: A Parametric Investigation

Noureddine Boucif, Jean Pierre Corriou, Denis Roizard, and Eric Favre
Laboratoire Réactions et Génie des Procédés LRGP (UPR 3349 CNRS) Nancy Université, BP 20451 - 1, rue Grandville, F-54001 Nancy Cedex, France

DOI 10.1002/aic.12791
Published online November 7, 2011 in Wiley Online Library (wileyonlinelibrary.com).

A mathematical and numerical investigations on the gas–liquid absorption of carbon dioxide in monoethanolamine solutions in a hollow fiber membrane contactor device is described. The reactive absorption mechanism was built based on momentum and mass transport conservation laws in all three compartments involved in the process, i.e., the gas phase, the membrane barrier, and the liquid phase. The liquid absorbing solution flows in the fiber bore in which the velocity is assumed to obey a fully developed laminar flow, and the gas mixture circulates counter-currently to the liquid flow in the shell side where the velocity is characterized by the Navier-Stokes momentum balance equations. The average outlet gas and liquid concentrations, the reactive absorption flux, and the gas removal efficiencies are parametrically simulated with operational parameters such as gas flow rate, fresh inlet amine concentrations, and fiber geometrical characteristics. The shell velocity was described by other flow hydrodynamics models besides Navier-Stokes and their simulated results were favorably compared to experimental data. © 2011 American Institute of Chemical Engineers *AIChE J,* 58: 2843–2855, 2012
Keywords: absorption, mathematical modeling, membrane separations, Navier-Stokes equations

Introduction

Carbon dioxide accounts for the major source responsible for global warming which is considered as the greatest environmental challenge the world is facing. The efforts to control the greenhouse gas emissions include the removal of CO_2 from flue gases. Membrane applications for gas–liquid separations have made such rapid developments that traditional methods of gas purification are being enhanced and in some cases replaced by membrane technologies. The removal of carbon dioxide from process gas streams is an important step in many industrial processes and is required because of environmental, economical or process technical reasons. In the presence of water, CO_2 being an acid gas can cause corrosion to process equipments. Besides this, the presence of CO_2 reduces the heating value of a natural gas stream and also causes the waste of valuable pipeline capacity. In liquefied natural gas (LNG) plants, carbon dioxide should be removed to prevent freezing in low-temperature chillers. Moreover, in the manufacture of ammonia, carbon dioxide would poison the reactor catalyst.

Furthermore, carbon dioxide resulting from fossil fuels based energy still represents more than 80% of the primary energy in use today, despite the increasing interest in renewable energy sources. Carbon dioxide resulting from these fossil fuels in power plant combustion represents the major contribution to greenhouse gas emissions. An urgent need for developing cost effective carbon dioxide capture and sequestration technologies is strongly motivated by the global climate warming and the causal link between these greenhouse gas emissions.

A variety of industrial techniques are presently available for the separation of carbon dioxide from flue gas streams such as packed bed absorption, molecular sieve adsorption, cryogenic distillation, and lately membrane diffusion. The most widely used technique for removing carbon dioxide is absorption into alkanolamines solutions in classical contactor equipments. However, besides occupying huge spaces, these processes require important initial investment costs. The membrane gas–liquid absorption process is day to day considered as an alternative process for carbon dioxide capture.

The hollow fiber gas–liquid contacting process, a hybrid process combining the advantages of both conventional reactive absorption and membrane contactor processes, is considered as an alternative technology which can potentially overcome the operational shortcomings encountered in traditional processes such as entrainment and flooding at high flowrates, and reduces considerably the foaming effects. The advantages of these hybrid processes over the conventional absorption ones depend closely on gas–liquid systems, types of membranes and operating conditions.

Besides providing a potentially high selectivity combined with a substantially high mass transfer driving force, the gas liquid hollow fiber membrane contactor supplies a knowable and high contacting surface area, independent control of both gas and liquid flow rates.[1] Because of their attractive characteristics, these contactors have been extensively investigated by many researchers since the early 70's and have driven considerable research in a wide range of applications. It is commonly recognized that Esato and Eiseman[2]

Correspondence concerning this article should be addressed to N. Boucif at Noureddine.Boucif@ensic.u-nancy.fr.

pioneered this technology being the first to use a flat polytetrafluoroethylene membrane as a gas–liquid contactor for a blood oxygenation device. A few years later, Tsuji et al.[3] applied a microporous hollow fiber made of polypropylene to oxygenate blood. Qi and Cussler[4] later used a microporous polypropylene membrane to absorb CO_2 in a NaOH solution. The earliest model of reactive gas-liquid absorption for SO_2 in hollow fiber membrane-based contactors has been provided by Karoor and Sirkar.[5,6] Moreover, these authors were the first to investigate the carbon dioxide removal by an aqueous alkanolamine solution (diethanolamine) in a microporous membrane-based contactor. Kreulen et al.[7,8] developed a model and simulated mass transfer in a hollow fiber contactor for gas–liquid absorption with and without chemical reaction. They used various gas-liquid systems (CO_2 in water/glycol and gas mixture of CO_2 in NaOH aqueous solutions) to investigate the effects of membrane porosity, module dimension and liquid viscosity. Feron et al.[9] performed experimental studies of the chemical absorption of CO_2 by specific absorbing solutions named CORAL (CO_2 removal absorption liquids) in a polyolefin membrane contactor. Theoretical studies of the chemical absorption of CO_2 in a polypropylene microporous hollow fiber membrane contactor using typical amine solutions (AMP, DEA, DIPA) have been conducted by Boucif et al.[10]

The gas absorption performance is considerably influenced by shell side channeling. Because the shell side flow pattern in the module is quite complex to quantify, it is usually simplified by making some assumptions which are practically verified for some special cases only. If the gas flowing in the shell side is assumed as a pure gas, the main mass transfer resistance may be related to liquid and membrane phase resistances. However, if the gas in the shell side is a mixture and chemically absorbed in the liquid solution, the gas phase resistance should be considered. Henceforth, in common cases, the channeling occurring in the module shell might have a substantial effect on the contactor performance, and consequently the shell side hydrodynamics ought to be taken into account.

A couple of theoretical models have been applied to characterize the shell side velocity for gas–liquid hollow fiber modules. Boucif et al.[11] used the plug flow model to evaluate both the axial velocity and concentration gradients in the contactor shell. Karoor and Sirkar[6] and recently Boucif et al.[12] employed the Happel's free surface model to estimate the shell side flow, assuming the fibers being regularly arranged in the shell side with a constant axial velocity in the contactor shell. The shell side fluid flow is usually characterized as a plug flow model or Happel's free surface theory, which represents some shortcomings due to the randomly spacing and arrangement of the fibers in the cartridge. Although these models are considered as a step ahead in the modeling of gas–liquid mass transfer in hollow fiber membrane, they still exhibit some weaknesses due to the assumption of the random spacing and arrangement of the fibers in the module shell compartment.

Computational fluid dynamics (CFD) could be an eligible tool to overcome these difficulties encountered in hydrodynamics modeling. It has been widely used to model various membrane separation processes. The Navier-Stokes equations were solved and numerical simulations were performed for membrane filtration,[13] microfiltration and ultraflitration,[14] nanofiltration and reverse osmosis.[15] Many researchers used this tool to investigate different membrane module configurations such as flat sheet,[16] rotating circular geometry[17] and tubular membrane with inserts.[18] Kieffer et al.[19] investigated mass transfer with chemical reaction in a liquid–liquid tubular membrane contactor and simulated the effects of different geometrical parameters on the module performance.

This work is an attempt to develop a mathematical model to numerically simulate the behavior of a gas–liquid hollow fiber membrane contactor using computational fluid dynamics (CFD) of momentum and mass transfer in the shell side at laminar flow conditions for both cocurrent and countercurrent flow patterns. The microscopic theoretical model includes second order reversible reactions of the soluble gas in the absorbent based on the two-step carbamate formation mechanism. The objective of this study is to validate the numerical simulations of a rigorous rate-based model for a solvent absorption process. The mass-transfer model is developed based on the momentum and mass conservation laws with special emphasis on implementing numerical mesh sizing that gives accurate and rapid convergence. The aim of the simulations is to predict the concentration profiles of both solute and solvent in all three contactors compartments. The influence of various operating parameters (gas and liquid velocities, inlet fresh gas and liquid concentrations) on the hollow fiber membrane contactor performance is investigated.

This article concentrates on the validation of the numerical simulations and a subsequent paper will focus on the fitting of laboratory data to be collected on an experimental rig. The developed model is written primarily for modeling CO_2 removal from postcombustion flue gas systems at atmospheric pressure, but can as well be used for modeling acid gas absorption from natural gas or other process streams.

Mathematical Model Formulation

Mass transport is considered in all three domains involved in the transfer process, i.e., the fiber side, the membrane wall and the shell side of the module in which gas and liquid concentrations are tied to each other at both fiber-inner wall and outer wall-shell frontiers by the appropriate boundary conditions. The model considers mass transport by convective diffusion of the gas first in the shell side (gas phase), then through the membrane pores, and finally in the fiber bore (liquid phase) where a reaction with the absorbing solution is taking place. The basic concept of this model is schematically explained in Figure 1. Although pumping the liquid through hollow fibers having small diameters is costly, it has been reported by many researchers[4,20] that the performance of running hollow fiber contactors with the liquid solution flowing in the fiber lumen and the gas mixture in the shell side is considerably higher than inverting the liquid and gas flows from fiber to shell and vice versa. This performance drop is thought to be caused by the serious liquid channeling in the contactor shell side. Although membrane-based hollow fiber contactors with gas flowing in the fiber bore are commercially the most successful, theoretical models with experimental setup designs[10,21–24] are usually developed for the liquid phase flowing in the fiber bore and the gas phase in the shell.

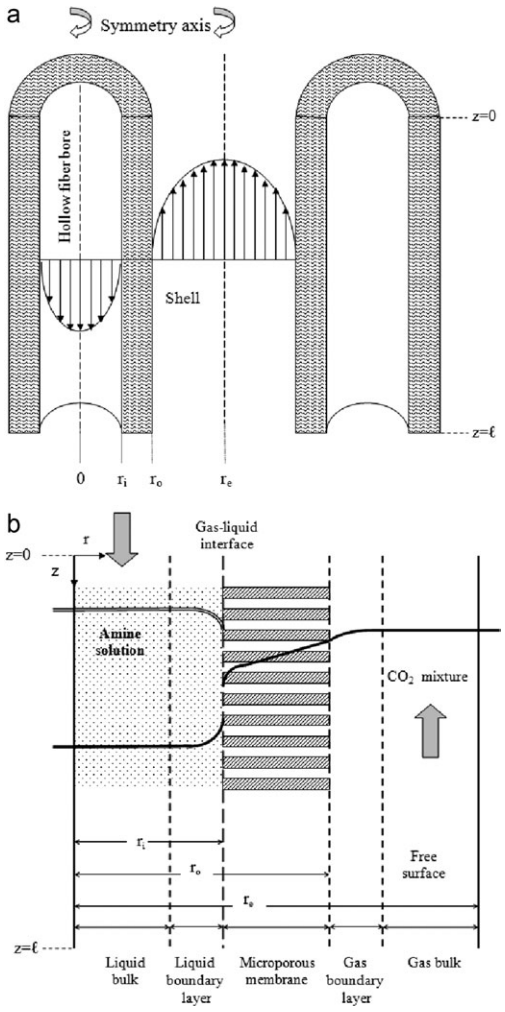

Figure 1. Three modeled domain and concentration profiles in a hollow fiber membrane contactor for a countercurrent flow regime.

Assumptions

The following assumptions are made to generate the governing equations of the CO_2 and the alkanolamine solution microscopic mass balances

- The steady state process is isothermal and the gas mixture is assumed to be ideal
- The axial diffusion is neglected in both tube and shell side
- The convective mass transfer in the gas-filled membrane pores is neglected
- The absorbent liquid is assumed to be an incompressible Newtonian fluid
- The absorbent liquid pressure drop in the shell side is neglected
- A fully developed concentration profile is assumed in the fiber
- Constant liquid viscosity and gas and liquid diffusivities

Mass balances in the three contactor areas for countercurrent flow regime

The module's hollow fiber membrane is split in three compartments as shown in Figure 1, and the corresponding mass balances in countercurrent flow regime have been set up.

(1) Fiber bore domain: In the fiber bore, the steady state CO_2 mass transfer by diffusion and convection accompanied by the chemical reaction is written as

$$v_{zf}\frac{\partial[CO_2]_f}{\partial z}=\frac{1}{r}\frac{\partial}{\partial r}\left[r\mathcal{D}_{CO_2f}\frac{\partial[CO_2]_f}{\partial r}\right]-\mathcal{R}_{CO_2} \tag{1}$$

$$v_{zf}\frac{\partial[Am]_f}{\partial z}=\frac{1}{r}\frac{\partial}{\partial r}\left[r\mathcal{D}_{Am}\frac{\partial[Am]_f}{\partial r}\right]-\mathcal{R}_{Am} \tag{2}$$

The liquid velocity in the fiber bore is assumed to obey a fully developed parabolic profile, i.e.

$$v_{zf}=2v_{zf}^0\left[1-\left(\frac{r}{r_i}\right)^2\right] \tag{3}$$

The term $\mathcal{R}_{CO_2}$ stands for the carbon dioxide reaction rate in the liquid phase. In aqueous solutions, primary, secondary and tertiary alkanolamines exhibit different behaviors towards CO_2 due to their molecular structure. Primary and secondary alkanolamines react with CO_2 producing carbamate species according to

$$CO_2+R_1R_2NH\rightleftharpoons R_1R_2NH^+COO^- \tag{4}$$

$$R_1R_2NH^+COO^-+R_1R_2NH\rightleftharpoons R_1R_2NH_2^++R_1R_2NCOO^- \tag{5}$$

leading to the generalized overall reaction

$$CO_2+2AmH\underset{k_{-1}}{\overset{k_1}{\rightleftharpoons}}AmH_2^++AmCOO^- \tag{6}$$

The reaction rate is based on the two step carbamate formation mechanism

$$\mathcal{R}_{CO_2}=\left[\frac{k_1}{1+\frac{k_{-1}}{k_{Am}[Am]_f}}\right]\left\{[CO_2]_f[Am]_f-\frac{\left[C_T-[Am]_f\right]^2}{4K_{eq}[Am]_f}\right\} \tag{7}$$

In the case of MEA, the term $k_{Am}[Am]_f$ is assumed to be very large[25] compared to k_{-1}. The reaction rate constant has been calculated from the expression derived by Hikita et al.[26] and is valid in the range of [5–80°C], and 0.0152–0.177 kg mol/m^3 follows the Arrhenius form as $k_1=A_R\exp\frac{-E_R}{RT_o}$, where the second order rate constant is $A_R=9.7744\times10^{10}$ m^3/mol s, and the activation energy $E_R=41197.53$ J/mol.

The governing mass transfer equations are subject to the following boundary conditions

$$\text{at } z=0,\qquad [CO_2]_f=0\qquad [Am]_f=C_T\quad \forall\, r_i\geq r\geq 0 \tag{8}$$

$$\text{at } r=0,\qquad \frac{\partial[CO_2]_f}{\partial r}=0\qquad \frac{\partial[Am]_f}{\partial r}=0\quad \forall\, l\geq z\geq 0 \tag{9}$$

$$\text{at } r=r_i,\quad [CO_2]_f=\mathcal{H}_{CO_2}[CO_2]_m\quad \frac{\partial[Am]_f}{\partial r}=0\quad \forall\, l\geq z\geq 0 \tag{10}$$

(2) Polymeric membrane domain: Through the hydrophobic membrane pores (assuming porosity higher than 10%), the steady state CO_2 mass transfer is assumed to be mainly diffusive and written as

$$\frac{1}{r}\frac{\partial}{\partial r}\left[r\mathcal{D}_{CO_2m}\frac{\partial[CO_2]_m}{\partial r}\right]=0 \tag{11}$$

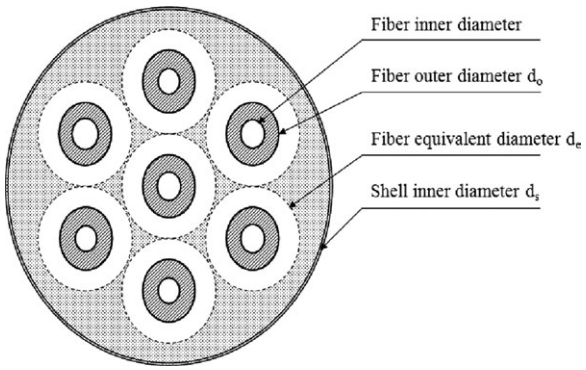

Figure 2. Circular approximately shaped fiber assembly bundle.

subject to the following boundary conditions

$$\text{at } r = r_i, \qquad [CO_2]_m = \frac{[CO_2]_f}{\mathcal{H}_{CO_2}} \qquad \forall\, l \geq z \geq 0 \tag{12}$$

$$\text{at } r = r_o, \qquad [CO_2]_m = [CO_2]_s \qquad \forall\, l \geq z \geq 0 \tag{13}$$

Furthermore, the carbon dioxide concentrations in the fiber bore $[CO_2]_f$, in the membrane pore $[CO_2]_m$ and in the shell side $[CO_2]_s$ are related to each other by the flux continuity equations at the fiber-membrane and at the membrane-shell boundaries as

$$\text{at } r = r_i, \quad \mathcal{D}_{CO_2 f} \frac{\partial [CO_2]_f}{\partial r} = \mathcal{D}_{CO_2 m} \partial [CO_2]_m \partial r \qquad \forall\, l \geq z \geq 0 \tag{14}$$

$$\text{at } r = r_o, \quad \mathcal{D}_{CO_2 m} \frac{\partial [CO_2]_m}{\partial r} = \mathcal{D}_{CO_2 s} \partial [CO_2]_s \partial r \qquad \forall\, l \geq z \geq 0 \tag{15}$$

(3) Shell domain: In the shell side, the steady state mass transfer by diffusion and convection is written as

$$v_{zs} \frac{\partial [CO_2]_s}{\partial z} = \frac{1}{r} \frac{\partial}{\partial r} \left[r \mathcal{D}_{CO_2 s} \frac{\partial [CO_2]_s}{\partial r} \right] \tag{16}$$

The velocity in the shell compartment could be characterized by various model equations assuming the fiber bundle assembled in a regular circular shape as shown in Figure 2.

• Plug flow: In the gas phase, a macroscopic mass balance characterizing the solute concentration gradient over the shell length is written as

$$\frac{v_{zs^0} d_s^2 (1 - \varphi)}{4 n d_o} \frac{d [CO_2]_s}{dz} = k_{CO_2 s} \left[[CO_2]_s - [CO_2]_s^{\text{int}} \right] \tag{17}$$

• Happel flow: The velocity in the shell domain is characterized by Happel free surface model described by the following equation

$$v_{zs} = 2 v_{zs}^0 \left[1 - \left(\frac{r_o}{r_e} \right)^2 \right] \left\{ \frac{\left(\frac{r}{r_e} \right)^2 - \left(\frac{r_o}{r_e} \right)^2 - \ln \left(\frac{r}{r_e} \right)^2}{3 + \left(\frac{r_o}{r_e} \right)^2 - 4 \left(\frac{r_o}{r_e} \right)^4 + \ln \left(\frac{r_o}{r_e} \right)^4} \right\} \tag{18}$$

where r_e stands for the free surface radius defined in terms of the packing fraction as $r_e = r_s\,(n_f)^{-0.5}$. The shell side volume fraction ε is easily calculated as $1 - n_f \left[\frac{r_o}{r_e} \right]$.

• Navier-Stokes flow:

$$\frac{1}{r} \frac{\partial}{\partial r} (r v_{rs}) + \frac{\partial v_{zs}}{\partial z} = 0 \tag{19}$$

$$\rho_{CO_2} \left[v_{rs} \frac{\partial v_{rs}}{\partial r} + v_{zs} \frac{\partial v_{rs}}{\partial z} \right] = \mu_{CO_2} \left[\frac{\partial}{\partial r} \left(\frac{1}{r} \frac{\partial}{\partial r} (r v_{rs}) \right) + \frac{\partial^2 v_{rs}}{\partial z^2} \right] \tag{20}$$

$$\rho_{CO_2} \left[v_{rs} \frac{\partial v_{zs}}{\partial r} + v_{zs} \frac{\partial v_{zs}}{\partial z} \right] = -\frac{\partial p}{\partial z} + \mu_{CO_2} \left[\frac{1}{r} \frac{\partial}{\partial r} \left(r \frac{\partial v_{zs}}{\partial r} \right) + \frac{\partial^2 v_{zs}}{\partial z^2} \right] \tag{21}$$

v_{rs} and v_{zs} are the velocities in the shell compartment with respect to r and z directions respectively. They are characterized by Navier-Stokes equations,[27] in which the continuity balance (19) is combined with the momentum balance (20) and (21) at steady state for an incompressible and Newtonian fluid.

If one assumes no slip condition at the outer fiber wall, the above differential equations are subject to the following boundary conditions

$$\text{at } z = 0, \qquad p = p_o = p_{in} \qquad \forall\, r_e \geq r \geq r_o \tag{22}$$

$$\text{at } r = r_o, \quad [CO_2]_s = [CO_2]_m \quad v_{rs} = 0 \quad v_{zs} = 0 \qquad \forall\, l \geq z \geq 0 \tag{23}$$

$$\text{at } r = r_e, \quad \frac{\partial [CO_2]_s}{\partial r} = 0 \quad v_{rs} = 0 \qquad v_{zs} = v_{zs}^0 \qquad \forall\, l \geq z \geq 0 \tag{24}$$

$$\text{at } z = l, \quad [CO_2]_s = [CO_2]_{in} \quad v_{rs} = 0 \quad v_{zs} = 0 \quad \forall\, r_e \geq r \geq r_o \tag{25}$$

The outlet gas concentrations, in the fiber bore and the shell, respectively, $[CO_2]_f$ and $[CO_2]_s$ are determined as mixing cup concentrations[28] given as

$$[CO_2]_{f,out} = \frac{\int_0^{r_i} 2\pi r v_{zf}(r) [CO_2]_f dr}{\int_0^{r_i} 2\pi r v_{zf}(r) dr} \tag{26}$$

$$[CO_2]_{s,out} = \frac{\int_{r_o}^{r_e} 2\pi r v_{zs} [CO_2]_s dr}{\int_{r_o}^{r_e} 2\pi r v_{zs} dr} \tag{27}$$

Mass Transport Theory

For a membrane module with a hydrophobic microporous membrane, the absorption accompanied by a chemical reaction is a three step process as described in Figure 1. The solute species is transferred from the gas phase to the internal pore mouth of the membrane, then through the membrane pores, and finally absorbed by the liquid solution where it reacts. As shown in Figure 1, and based on the driving forces of the concentration differences, the molar mass transfer flux J_{CO_2} of solute per unit area is depicted as:

$$
\begin{aligned}
J_{CO_2} &= k_{CO_2s}([CO_2]_s - [CO_2]_m) \\
&= k_{CO_2m}([CO_2]_m - [CO_2]_f^{int}) \\
&= k_{CO_2f}([CO_2]_f^{int} - [CO_2]_f) \\
&= K_{ov}\, A_T\, \Delta[CO_2]_{lm}
\end{aligned} \tag{28}
$$

Writing a component mass balance over the membrane module, assuming no change in both gas and liquid flow rates, the inlet absorbent being a fresh amine solution, i.e.

$$
V[CO_2]_{in} - V[CO_2]_{out} = L[Am]_{out} \tag{29}
$$

The logarithmic mean difference $\Delta[CO_2]_{out}$ (30) is expressed analogically to heat transfer[29] as

$$
\Delta[CO_2]_{lm} = \frac{([CO_2]_{f,out}^{int} - [CO_2]_{f,out}) - ([CO_2]_{f,in}^{int} - [CO_2]_{f,in})}{\ln\left[\frac{[CO_2]_{f,out}^{int} - [CO_2]_{f,out}}{[CO_2]_{f,in}^{int} - [CO_2]_{f,in}}\right]} \tag{30}
$$

where $[CO_2]_{f,in}^{int}$ and $[CO_2]_{f,out}^{int}$ are the concentrations of the solvent solution at the gas–liquid interface of the membrane wall. Introducing Henry's law to estimate the liquid concentrations at the gas liquid interface, i.e., $[CO_2]_{f,in}^{int} = \mathcal{H}_{CO_2}[CO_2]_{s,in}$ and $[CO_2]_{f,out}^{int} = \mathcal{H}_{CO_2}[CO_2]_{s,out}$, after substitution and rearrangements it yields

$$
K_{ov} = \frac{L[CO_2]_{f,out} \ln\left[\frac{\mathcal{H}_{CO_2}[CO_2]_{s,out}}{\mathcal{H}_{CO_2}[CO_2]_{s,in} - [CO_2]_{f,out}}\right]}{A_T\left[\mathcal{H}_{CO_2}[CO_2]_{s,out} - (\mathcal{H}_{CO_2}[CO_2]_{s,in} - [CO_2]_{f,out})\right]} \tag{31}
$$

Overall mass transfer

For a hydrophobic membrane with gas filled pores and liquid flowing in the fiber, the liquid phase based driving force overall mass transfer coefficient K_{ov} is also expressed as resistances in series, usually related to mass transfer resistances in the three phases, for a hydrophobic membrane with gas filled pores and liquid flowing in the fiber[1]

$$
\frac{1}{K_{ov}} = \frac{d_i}{d_o \mathcal{H}_{CO_2} k_{CO_2s}} + \frac{d_i}{d_{lm} \mathcal{H}_{CO_2} k_{CO_2m}} + \frac{1}{E k_{CO_2f}} \tag{32}
$$

Mass transfer in the fiber bore

The liquid phase mass-transfer coefficient in the fiber, k_{CO_2f}, could be determined by the correlation suggested by Kreulen et al.[7] valid over a very wide range of Graetz numbers

$$
Sh_{Af} = \frac{k_{CO_2f} d_i}{\mathcal{D}_{CO_2f}} = [(3.67^3) + (1.62^3 Gr_{Af})]^{1/3} \tag{33}
$$

Mass transfer through the membrane

The resistance to mass transfer through the membrane depends on the nature of that polymeric barrier. Two types of membrane are used in this study, namely a polypropylene (PP) which is a microporous membrane and a polydimethylsiloxane (PDMS) which is a dense membrane.

Microporous Membrane. The resistance to mass transfer within a hydrophobic microporous membrane (PP), which is mainly due to the membrane structure and the presence of a stagnant film within the pores, is usually described by Fick's law and expressed as

$$
\frac{1}{k_{CO_2m}} = \frac{\delta\tau}{\varepsilon \mathcal{D}_{CO_2m}} = \frac{\delta\tau}{\varepsilon}\left[\frac{1}{\mathcal{D}_{CO_2s}} + \frac{1}{\mathcal{D}_{CO_2K}}\right] \tag{34}
$$

The tortuosity has been related to the porosity by[30] as $\tau = \frac{(2-\varepsilon)^2}{\varepsilon}$. $\mathcal{D}_{CO_2m}$ is the effective diffusion coefficient in the membrane gas filled pores, and is a combination of the continuum diffusion $\mathcal{D}_{CO_2s}$ which is determined by the different molecules interactions, and the Knudsen diffusion $\mathcal{D}_{CO_2K}$ which takes into account the molecules interactions within the pore wall. The Knudsen diffusion is expressed as $\mathcal{D}_{CO_2K} = \left[\frac{3r_p}{3}\right]\sqrt{\frac{8RT}{\pi M_{CO_2}}}$, which is temperature dependent.

Dense Membrane. The resistance to mass transfer within dense membranes (PDMS) k_{CO_2m} is usually experimentally estimated. The dense membrane is a composite material made out of a porous support coated internally with a PDMS thin layer, in which the polymer coating constitutes the main resistance to mass transport. The permeability of the dense polymeric membrane is the product of the diffusivity and the solubility of the gas $P = DS$.

The physical properties of the CO_2/MEA are listed in Table 2.

Mass transfer in the shell cartridge

The gas phase mass-transfer coefficient in the shell side k_{CO_2s}, has been correlated depending on the nature of the flow regime. For laminar flow regime ($Re < 2100$)[31]

$$
Sh_{As} = \frac{k_{CO_2s} d_e}{\mathcal{D}_{CO_2s}} = 1.25\left[\frac{d_e}{l} Re_{As}\right]^{0.93}\left[Sh_{As}\right]^{\frac{1}{3}} \tag{35}
$$

For transitional flow regime ($2100 < Re < 10{,}000$)[32]

$$
Sh_{As} = \frac{k_{CO_2s} d_e}{\mathcal{D}_{CO_2s}} = 0.116\left[Re_{As}^{\frac{2}{3}} - 125\right]\left[1 + \left[\frac{d_e}{l}\right]^{\frac{2}{3}}\right] \tag{36}
$$

For turbulent flow regime ($Re > 10{,}000$)[32]

$$
Sh_{As} = \frac{k_{CO_2s} d_e}{\mathcal{D}_{CO_2s}} = 0.023 Re_{As}^{0.8} Sh_{As}^{\frac{2}{3}} \tag{37}
$$

As per Sh_{As}, both Re_{As} and Sc_{As} are based on the equivalent diameter defined as $d_e = d_s\,(n_f)^{-0.5}$

Enhancement factor

The enhancement factor E expresses the effect of the chemical reaction on the absorption and is defined as the ratio of the chemically enhanced over the physical absorption fluxes at identical driving forces. For a mass transport accompanied by an irreversible second order chemical reaction, the enhancement factor E is determined as[33]

$$
E = \frac{-Ha^2}{2(E_\infty - 1)} + \left[\frac{Ha^2}{4(E_\infty - 1)^2} + \frac{E_\infty Ha^2}{(E_\infty - 1)} + 1\right]^{\frac{1}{2}} \tag{38}
$$

where Ha stands for the Hatta number and E_∞ is the asymptotically infinite enhancement factor

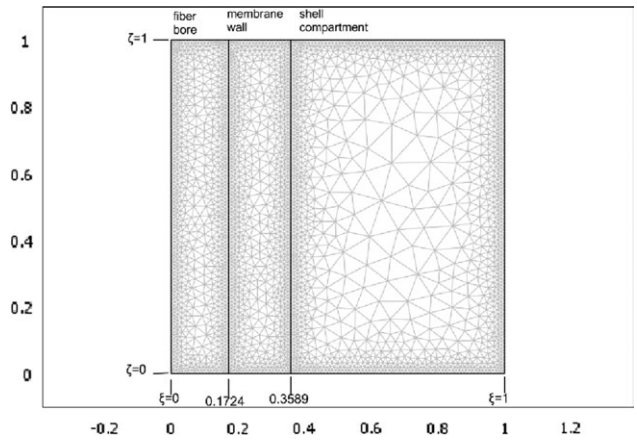

Figure 3. Contactor compartments sizing and mesh discretization for the dense membrane.

$$E_\infty = 1 + \frac{Ha[\mathrm{Am}]_{\mathrm{in}}}{2[\mathrm{CO_2}]_{\mathrm{f}}^{\mathrm{int}}}\left[\frac{\mathcal{D}_{\mathrm{Amf}}}{\mathcal{D}_{\mathrm{CO_2f}}}\right]^{\frac{1}{2}} \tag{39}$$

For a reactive system of CO_2 with alkanolamines, *Ha* is expressed as

$$Ha = \frac{\left[k_{\mathrm{ov}}[\mathrm{Am}]_{\mathrm{in}}\mathcal{D}_{\mathrm{CO_2f}}\right]^{\frac{1}{2}}}{k_{\mathrm{CO_2f}}} \tag{40}$$

Results and Discussion

The model equations, rewritten in dimensionless form and listed in Appendix, were solved using the direct linear system solver UMFPACK of COMSOL Multiphysics Modeling version 3.5, a very friendly used software package licensed from COMSOL, Burlington, MA. COMSOL Multiphysics Modeling, a powerful computer software, uses the finite element method to solve fluid flow, mass and heat transport, as well as many other engineering problems. A comprehensive account of COMSOL Multiphysics Modeling is available in literature.[34] Very recently, an extensive overview of many of the choices provided by this software has been presented by Finlayson,[35] by means of different illustrations on how to solve complicated problems.

The description of hollow fiber systems by analytical solutions, which are usually good tools, is limited in some cases, such as considering the bulk volume adjacent to the mass transfer zone being well mixed. This is actually not true for small membrane fiber diameters. For long residence time (i.e., low *Gz* numbers), the mass transfer zone in the liquid phase of the hollow fiber may extend up to the axis of the fiber. Such difficulties are overcome by the CFD based modeling techniques.

The hardware used to run the simulations is a CPU 2.4 GHz Pentium Personal Computer with a 2.0 GB RAM processor. Each hollow fiber has been discretized into 22,334 finite elements with a thicker mesh in the dense layer and the CPU solution time is 192.68 s for 129,701 degrees of freedom solved for. Figure 3 displays the triangular element shape discretization of all three compartments for the dimensionless configuration adopted in these numerical simulations. The dimensions of the hollow fiber membrane contactors studied in this paper are reported in Table 1, and the CO_2-MEA system obeys the physico-chemical parameters listed in Table 2. Besides, it is worth to point out that all simulations were performed for a contactor run in a countercurrent flow pattern except in Figure 5.

Velocity profiles

The velocity in the gas phase plays an important role in the design of gas–liquid absorbers made of hollow fibers. Figure 4 represents the dimensionless velocity profiles in the fiber lumen where the solvent is flowing as well as the profile in the shell region where the gas solute circulates counter-currently with respect to the liquid flow. It is clearly observed that the fiber velocity profile obeys a parabolic behavior whereas the shell velocity is almost parabolic with a mean average velocity increasing when moving towards the contactor exit.

Concentration profiles

The numerically simulated dimensionless carbon dioxide concentrations are represented in Figure 5, for cocurrent and countercurrent flow regimes, respectively, in all three compartments in which the solute specie is involved, i.e., the fiber bore, the membrane barrier and the shell side. The solvent is admitted to the fiber lumen of the contactor where the solute concentration Φ_A is assumed zero, whereas the gas mixture enters the module at its maximum solute concentration (at $\zeta = 0$ for the cocurrent flow pattern and at $\zeta = 1$ for the countercurrent one). Due to the concentration difference, and as the gas stream flows through the shell, the solute is moving toward the membrane at the pore mouth of which it is absorbed by the moving solvent. Because the solute concentration is influenced by both diffusion and convection in both fiber and shell domains, it is represented in terms of both radial and axial coordinates, whereas in the membrane, only the radial concentration is shown. Assuming the reaction is pseudo first order, for the case $2 < Ha < E_\infty$ as detailed in[33] and,[36] both solvent and solute concentrations stay practically unchanged in the fiber domain and the depletion of the reactant at the fiber wall is negligible as shown in Figure 5. Furthermore, it is observed in Figure 5 that the solute concentration undergoes at the contactor exit at ($\zeta = 1$ for the cocurrent flow pattern and at $\zeta = 0$ for the countercurrent one) a sharp decay in the shell domain, then a relatively smooth decrease through the membrane to completely disappear in the fiber where it reacts and is absorbed by the solvent. The reason of such a behavior is that the solute

Table 1. Specifications of the Hollow Fiber Contactors Used in this Study

Characteristics	Module 1	Module 2
Fibers material	PDMS	PP
Polymer nature	Dense	Microporous
Fiber inner diameter in (μm)	305	280
Fiber outer diameter in (μm)	635	380
Thickness δ in (μm)	165	50
Average pore size r_p in (μm)		0.6
Porosity ε		0.4
Tortuosity $\tau = \tau = \frac{(2-\varepsilon)^2}{\varepsilon}$	–	6.4
Number of fibers n_f	54	54
Active module length in (mm)	240	240
Shell inner diameter (mm)	13	13
Fiber inner contact area in (10^{-6} m^2)	12.411	11.394
Fiber outer contact area in (10^{-6} m^2)	25.841	15.464
Packing fraction ϕ	0.128	0.046

Table 2. Physico-Chemical Parameters of the CO_2-MEA Chemical Absorption at 298.14 K

Designation	Symbol	Value	Source
Reaction rate constant (m^3/mol s)	k_1	$\frac{10^{10.99-\frac{2152}{T}}}{1000}$	26
Equilibrium constant (m^3/mol)	K_{eq}	172.97	26
Dimensionless partition coefficient	$m = \frac{1}{\mathcal{H}_{CO_2}}$	$\frac{2.82\times10^6}{RT}\exp\left[-\frac{2044}{T}\right]$	38
Diffusivity of CO_2 in the fiber (m^2/s)	$\mathcal{D}_{CO_2f}$	$2.35\times10^{-6}\exp\left[-\frac{2199}{T}\right]$	32
Diffusivity of CO_2 in microporous membrane (m^2/s)	$\mathcal{D}_{CO_2m}$	$1.855\times10^{-5}\left[\frac{\varepsilon}{\tau}\right]$	32
Diffusivity of CO_2 in dense membrane (m^2/s)	$\mathcal{D}_{CO_2m}$	1.07×10^{-9}	32
Permeability of CO_2 in dense membrane (Barrer*)	P_{CO_2m}	3230	39,1
Diffusivity of CO_2 in the shell (m^2/s)	$\mathcal{D}_{CO_2s}$	1.855×10^{-5}	38
Diffusivity of the amine in the fiber (m^2/s)	$\mathcal{D}_{Amf}$	$\exp\left[-13.275-\frac{2198.5}{T}\right]$	40
Kinematic viscosity of CO_2 (m^2/s)	η_{CO_2}	73.98×10^{-6}	41

*1 Barrer $= 10^{-10}\frac{cm^3\ (STP)\ cm}{cm^2\ s\ cmHg}$.

diffusion coefficient in the fiber lumen is much lower than those in both the membrane and shell compartments. Consequently, the solute mass transfer encounters a much lower resistance in the gas phase within the shell side than those in the membrane and the liquid phase flowing in the fiber bore. The effect of the gas flow rate on the removal efficiency is attributed to increasing concentration gradients within the fiber because radial diffusion length decreases with increasing flow rates (increasing Gz numbers).

Figure 6 displays the evolution of the radial carbon dioxide dimensionless concentration in the shell compartment at various longitudinal positions for a contactor run in a countercurrent regime. It is clearly seen that at the beginning of the absorption process (near the contactor entrance $\zeta = 1$), the bulk phase concentration is flat and remains almost unchanged up to a certain axial distance from which it starts reducing gradually. Then the solute concentration starts a uniform decay while moving towards the contactor exit ($\zeta = 0$). Figure 7 shows the axial solute concentration at different radial positions in the shell domain. It is observed that at $\xi = \lambda_2$, the dimensionless concentration decline is smooth, whereas the decay is getting sharper while moving towards the external frontier $\xi = 1$. This is mainly due to the formation of a gas boundary layer around the external membrane surface which transmits the diffusive resistance to carbon dioxide.

Influence of flow rates

The gas velocity is probably the most important operating variable in membrane gas–liquid contactors because of its considerable influence on the absorption flux. Figure 8 displays the evolution of the dimensionless CO_2 concentration along the contactor in the shell compartment at different gas velocities. As expected, the solute concentration in the shell decreases along the fiber length when the gas velocity decreases as a result of a longer residence time in the contactor.

The dependency of the carbon dioxide absorption flux on the gas flow velocities (transport convection term) along the length of the module is displayed in Figure 9. It is clearly observed that the CO_2 flux is zero at the shell contactor inlet and increases while moving toward the exit. Also, the carbon dioxide flux increases for increasing gas flow velocities. This is very likely due to the rise of the gas phase CO_2 concentration at the gas–liquid interface as a result of the low gas retention time. The sharpness of the rising and asymptotic trend

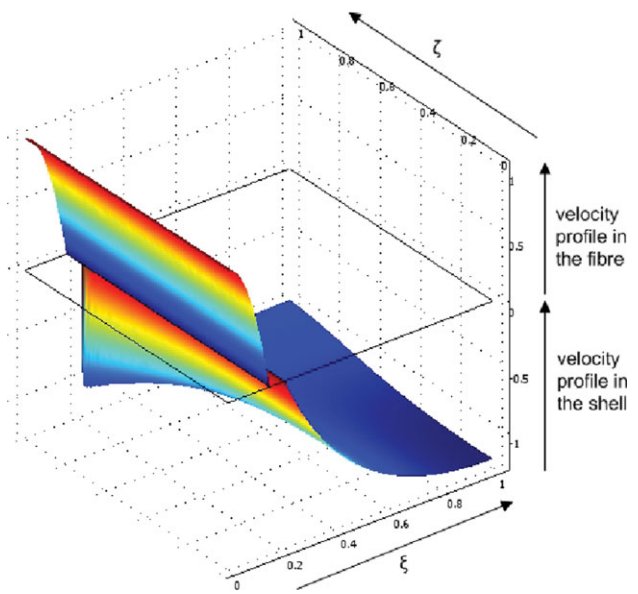

Figure 4. 3D Velocity profile in the lumen and shell sides of the dense membrane contactor ($[CO_2]_{in}$ = 5 mol/m^3, C_T = 1200 mol/m^3, v^0_{zf} = 0.42 m/s, v^0_{zs} = 0.014 m/s).

[Color figure can be viewed in the online issue, which is available at wileyonlinelibrary.com.]

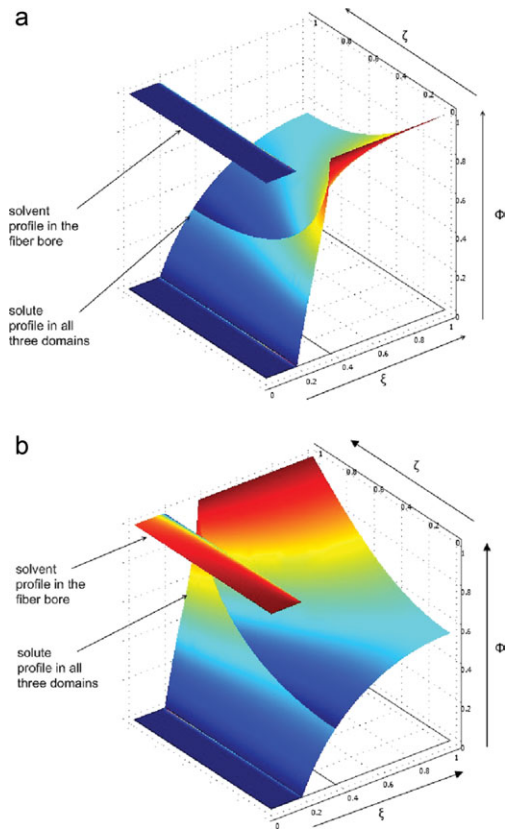

Figure 5. 3D Solute concentration profile in the lumen, membrane and shell sides of the dense membrane contactor for both flow regimes ($[CO_2]_{in}$ = 5 mol/m^3, C_T = 1200 mol/m^3, v^0_{zf} = 0.42 m/s, v^0_{zs} = 0.014 m/s). Left: cocurrent. Right: counter-current.

[Color figure can be viewed in the online issue, which is available at wileyonlinelibrary.com.]

diminishes gradually when lower gas velocities are applied. Furthermore, the CO_2 absorption flux J_{CO_2} is large for higher gas flow velocities. This is due to the fact that the solute concentration at the gas–liquid interface is high as a result of the small gas retention time. The gas phase mass transfer resistance is somehow low in general (around 10%), whereas both other resistances (membrane and liquid) share the remaining 90% in very variable proportions depending on the membrane's nature as well as the liquid side hydrodynamics.

Figure 10 depicts the dependency of the dimensionless carbon dioxide concentration on gas velocities for hollow fiber contactors made of dense or microporous membranes. A comparison in the absorption performances of both membranes modules has been made in terms of removal efficiency. An increase in the gas flow rate reduces the residence time in the contactor as expected and consequently the carbon dioxide removal rate. The CO_2 removal decreases from 92% to 60% in the dense membrane and from 78% to 57% in the microporous membrane when the gas velocity increases from 0 to 1 m/s. It is observed that at similar operating conditions, the solute recovery in the gas stream Ψ_{Aso} is lower for the PDMS membrane than for the PP one. The low removal rate occurring for the dense membrane made module is believed to be the result of the effect of the membrane resistance in the additional resistances as detailed in

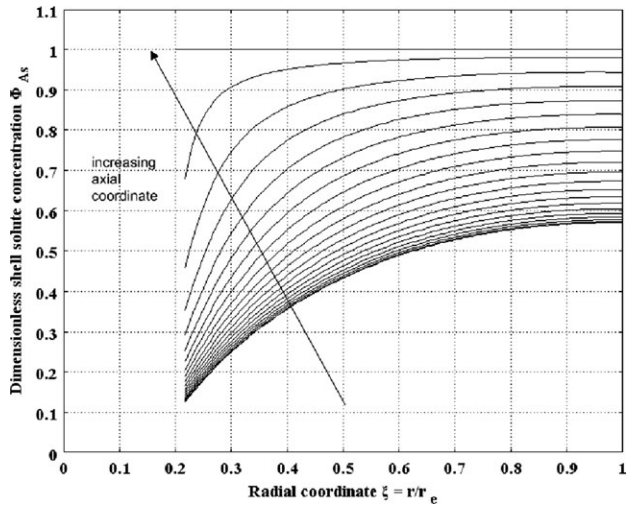

Figure 6. Shell solute concentration in the radial direction at various axial points in the microporous membrane contactor ($[CO_2]_{in}$ = 5 mol/m^3, C_T = 1200 mol/m^3, v^0_{zf} = 0.50 m/s, v^0_{zs} = 0.013 m/s, $\Delta\zeta$ = 0.05).

Eq. 32. Besides, it is worth mentioning that the simulation runs on liquid flow rate have shown a non noticeable effect of this latter on the solute removal.

The effluent concentrations of the PP membrane are significantly lower compared to the PDMS membrane at similar velocities, although the average residence time of the PP is almost similar to that of the PDMS (Table 1). Furthermore, the model was run for all three flow hydrodynamics, i.e., plug-flow, Happel free surface and Navier-Stokes models. The simulated absorption efficiencies are drawn in the same graphic (Figure 11) and confronted to experimental results taken from Nguyen thesis[37] for the microporous membrane module. Although the free surface model fits well the experimental data, it is clearly observed that these latter are in a better agreement with the Navier-Stokes model rather than with the two others.

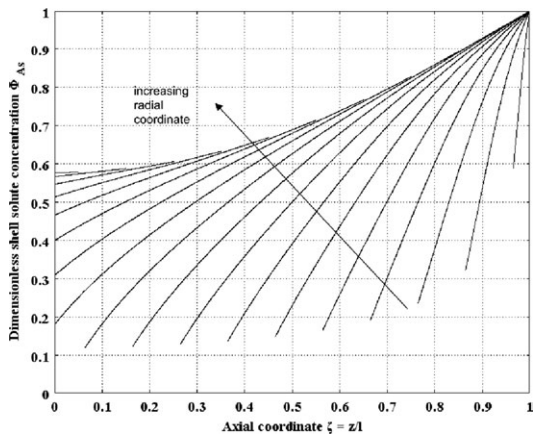

Figure 7. Shell solute concentration in the axial direction at various radial points in the microporous membrane contactor ($[CO_2]_{in}$ = 5 mol/m^3, C_T = 1200 mol/m^3, v^0_{zf} = 0.50 m/s, v^0_{zs} = 0.013 m/s, $\Delta\xi$ = 0.05).

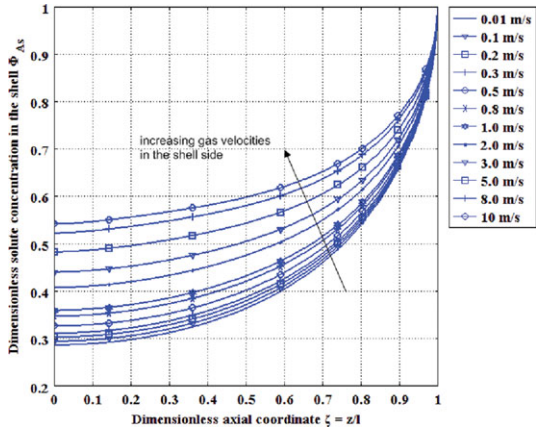

Figure 8. Solute concentration along the contactor length at various gas velocities in the dense membrane contactor ($[CO_2]_{in}$ = 5 mol/m^3, C_T = 1200 mol/m^3, v^0_{zf} = 0.42 m/s).

[Color figure can be viewed in the online issue, which is available at wileyonlinelibrary.com.]

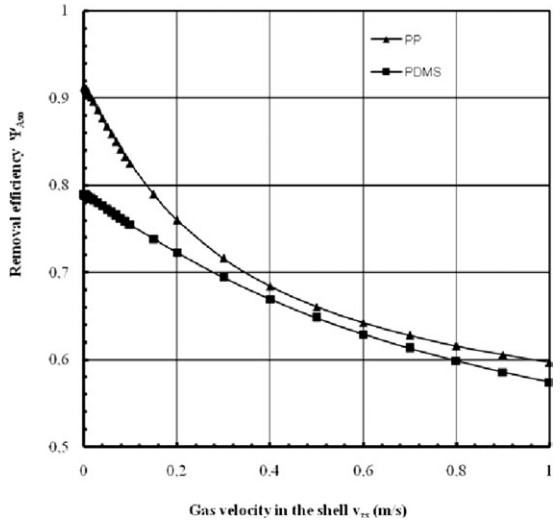

Figure 10. Effect of gas velocity on the removal efficiency for both PDMS and PP membrane made modules ($[CO_2]_{in}$ = 5 mol/m^3, C_T = 1200 mol/m^3, v^0_{zf} = 0.42 m/s).

Influence of MEA inlet concentration

The MEA is of common use in the chemical industry of carbon dioxide removal. It is universally accepted that the high reactivity of that alkanolamine with the carbon dioxide is of considerable advantage. However, its intensive corrosiveness to steel made process equipments represents a considerable shortcoming especially at high concentrations. Consequently, fairly diluted aqueous amine solutions are used in industrial carbon dioxide removal processes to avoid the solvent material corrosiveness and to take advantage of the solvent high reactivity to enhance mass transfer.

In Figure 12, the dimensionless outlet MEA concentration in the fiber is plotted as a function of the total inlet amine concentration. The carbon dioxide absorption seems to be substantially enhanced when the initial concentration of the absorbent solution is increased until saturation is reached beyond a value greater that 10^3 mol/m^3. Nevertheless, it must reminded that higher absorbent concentration could have harmful side-effects and cause irreversible damages to the hollow fiber membrane material as well as corrosion in the other metallic components. The carbon dioxide absorption being essentially limited by the reaction kinetics, the choice of the optimal inlet amine concentration is therefore dictated by a compromise among these operating requirements. The absorption system based on PP fiber have probably been condemned from being used as a practical application because of the pore wetting by the volatile amine. The use of other non volatile amine systems would be useful for understanding this application.

Influence of fiber dimensions

The carbon dioxide removal efficiency Ψ_{Aso} in the gas phase is plotted as a function of the hollow fiber module

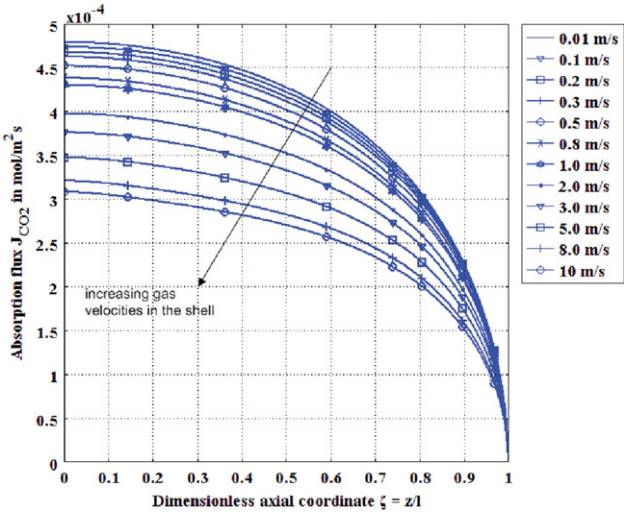

Figure 9. Absorption flux at different gas velocities for the dense membrane made contactor ($[CO_2]_{in}$ = 5 mol/m^3, C_T = 1200 mol/m^3, v^0_{zf} = 0.42 m/s).

[Color figure can be viewed in the online issue, which is available at wileyonlinelibrary. com.]

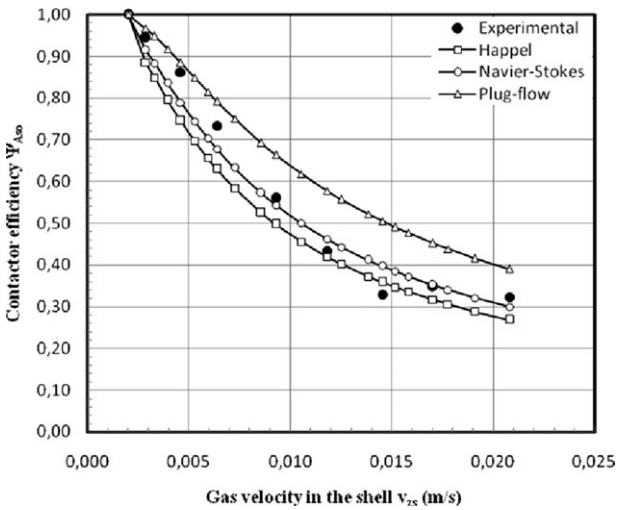

Figure 11. Comparison of contactor efficiencies using three shell side flow models for the microporous membrane contactor ($[CO_2]_{in}$ = 12.1 mol/m^3, C_T = 3292 mol/m^3, v^0_{zf} = 0.42 m/s).

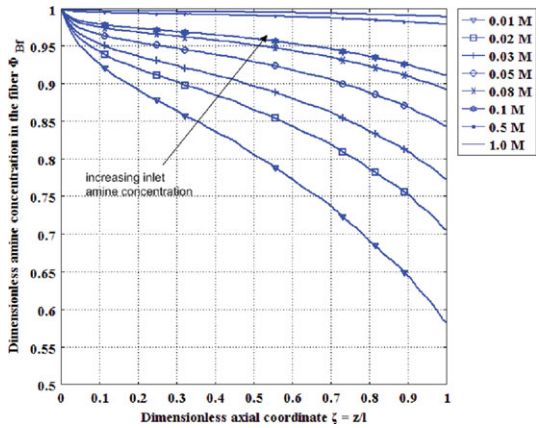

Figure 12. Axial alkanolamine concentration profile at various fresh solvent concentrations for the dense membrane contactor ($[CO_2]_{in}$ = 5 mol/m^3, $v^0_{zf} = 0.42$ m/s, $v^0_{zs} = 0.014$ m/s).

[Color figure can be viewed in the online issue, which is available at wileyonlinelibrary.com.]

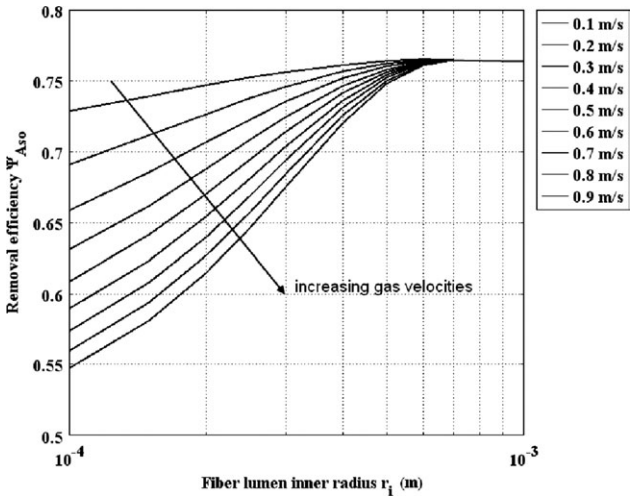

Figure 14. Effect of fiber inner radius on the removal efficiency at various gas velocities for the dense membrane contactor ($[CO_2]_{in}$ = 5 mol/m^3, C_T = 1200 mol/m^3, $v^0_{zf} = 0.42$ m/s).

length at different gas velocities in Figure 13. The initial amine concentration, solute concentration and liquid velocity are kept constant in these numerical simulations. The contactor performance is improved as the module length is increased until a point beyond which the removal efficiency is unaffected. However, the figure shows that for longer modules the absorption efficiency increases further as the gas velocity is increased. This is because for shorter fiber modules the residence time is short enough resulting in a solute richer gas at the module exit.

Figure 14 plots the gas phase carbon dioxide removal efficiency as a function of the hollow fiber lumen inner radius at different gas velocities. The fiber thickness has been kept constant for all the radii for which these simulations have been run. These results suggest that, for the same gas velocity, the removal efficiency is improved when larger fiber inner radii are employed in that range of gas velocities. This is obviously due to the fact that the removal efficiency is directly proportional to the interfacial area. However, this dependency is limited by the maximum number of fibers of the largest possible radius that could be embedded in a shell having the same dimensions.

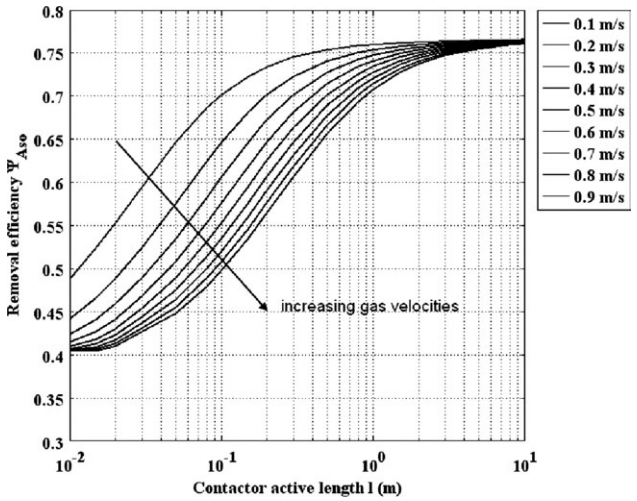

Figure 13. Effect of contactor length on the removal efficiency at various gas velocities for the dense membrane contactor ($[CO_2]_{in}$ = 5 mol/m^3, C_T = 1200 mol/m^3, $v^0_{zf} = 0.42$ m/s).

Conclusion

The chemical absorption of carbon dioxide in alkanolamines in hollow fiber membrane contactors is systematically investigated in the present work. A rigorous model consisting of a set of highly non-linear partial differential equations is rewritten in dimensionless form and numerically solved. Substantial variations in the radial and axial concentrations have been observed in all three compartments of the membrane modules for constant average velocities in the fiber lumen and shell side. The gas flow rate and the inlet solvent concentration influences on the contactor performance have been thoroughly studied. The carbon dioxide removal is substantially increased with decreasing the gas velocity in the shell side, whereas the liquid velocity variations in the fiber bore have not shown any noticeable effect. A comparison of microporous and nonporous membrane made hollow fiber contactors at identical operating parameters has shown higher performance for the microporous membrane module. Describing the shell domain gas velocity by plug-flow, Happel free surface and Navier-Stokes models reveals that the latter fits better the experimental results. Furthermore, the analysis of the simulation results reveals that the performance of the hollow fiber membrane contactor is dependent on the gas velocity in the fiber lumen as well as on the module's geometry.

Part of this material was presented at the international symposium ISCRE21 held in Philadelphia on June 13-16, 2010.

Notation

A_T = total surface area of gas liquid contact, m^2
A_C = shell cross sectional area, m^2
C_T = total fresh amine concentration, mol/m^3
$\mathcal{D}_i$ = diffusion coefficient of specie, m^2/s

d_i, d_o, d_e = inner, outer and equivalent fiber diameters, m
E = enhancement factor
Gr_i = dimensionless Graetz number of i specie
$\mathcal{H}_{CO_2}$ = dimensionless Henry's law constant
Ha = dimensionless Hatta number
J_i = molar mass transfer flux of specie i, mol/s
$\mathcal{J}_{CO_2}$ = average CO_2 absorption flux, mol/m^2 s
k_i = mass transfer coefficient of specie i, m/s
k_{Am} = forward second order reaction rate constant, m^3/mol s
k_{-1}, k_1 = forward and reverse second order reaction rate constant, m^3/mol s
k_{ov} = overall reaction rate constant based, m^3/mol s
K_{eq} = equilibrium constant
K_{ov} = overall mass transfer coefficient (m/s)
L = volumetric liquid flow rate (m^3/s)
l = active membrane fiber length (m)
m = partition coefficient
M_{CO_2} = solute molecular weight (kg/mol)
n_f = number of fibers in the bundle
p_{in} = inlet shell side pressure
r = radial coordinate
r_i, r_o, r_e = inner, outer and equivalent fiber radii (m)
r_p = mean pore radius (m)
Re_i = Reynolds number of specie i
$\mathcal{R}$ = ideal gas constant
Sc_i = dimensionless Schmidt number of specie i
Sh_i = dimensionless Sherwood number of specie i
T = temperature in (K)
V = volumetric gas flow rate (m^3/s)
v_{rs} = r dependent velocity in the shell
v_{zs} = z dependent velocity in the shell
v^0_{zf}, v^0_{zs} = mean average velocities in the fiber and shell in the z direction (m/s)
z = axial contactor coordinate

Greek symbols

β_i = dimensionless kinetics parameters
δ = membrane thickness
ε = membrane porosity
ζ = dimensionless longitudinal coordinate
η = liquid solution kinematic viscosity (m^2/s)
μ = liquid solution dynamic viscosity (kg/m s)
ξ = dimensionless radial coordinate in the fiber domain
ρ = liquid solution density (kg/m^3)
τ = membrane pore tortuosity
Φ_i = dimensionless concentration of specie i
ϕ = fiber bundle to shell void fraction
Ψ_i = removal of specie i

Subscripts and superscripts

int = interface
f = fiber
m = membrane
s = shell
0 = average
A = solute
B = solvent

Literature Cited

1. Ho WSW, Sirkar KK, editors. *Membrane Handbook*. New York: Van Nostrand Reinhold, 1992.
2. Esato K, Eiseman B. Experimental evaluation of gore-tex membrane oxygenator. *J Thorac Cardiovas Surg*. 1975;69:690–697.
3. Tsuji T, Suma K, Tanishita K, Fukazawa Z, Kanno M, Hasegawa H, Takahashi A. Development and clinical evaluation of hollow fiber membrane oxygenator. *Trans Am Soc Artif Intern Organs*. 1981; 27:280–284.
4. Qi Z, Cussler EL. Microporous Hollow fibers for gas absorption. Part I: mass transfer in the liquid. *J Membr Sci*. 1985; 23:321–332.
5. Karoor S. Gas absorption using microporous hollow fiber membranes. Ph.D. thesis, Stevens Institute of Technology, Hoboken, NJ, 1992.
6. Karoor S, Sirkar KK. Gas absorption studies in microporous hollow fiber membranes. *Ind Eng Chem Res*. 1993;32:674–684.
7. Kreulen H, Smolders CA, Versteeg GF, van Swaaij WPM. Microporous hollow fiber membrane modules as gas-liquid contactors. Part I: physical mass transfer processes, a specific application: mass transfer in highly viscous liquids. *J Membr Sci*. 1993;78: 197–216.
8. Kreulen H, Smolders C, Versteeg G, van Swaaij W. microporous hollow fiber membrane modules as gas-liquid contactors. Part II: mass transfer with chemical reaction. *J Membr Sci*. 1993;78:217–238.
9. Feron PHM, Jansen AE. CO_2 separation with polyolefin membrane contactors and dedicated absorption liquids: performance and prospects. *Sep Pur Technol*. 2002;27:231–242.
10. Boucif N, Favre E, Roizard D. CO_2 capture in HFMM contactor with typical amine solutions: a numerical analysis. *Chem Eng Sci*. 2008;63:5375–5385.
11. Boucif N, Nguyen PT, Roizard D, Favre E. Theoretical studies on carbon dioxide removal from a gas stream in hollow fiber membrane contactors. *Des Wat Treat*. 2010;14:146–157.
12. Boucif N, Roizard D, Favre E. Thermal effects on gas-liquid absorption in a hollow fiber membrane contactor: case of carbon dioxide in a monoethanoalmine solution. Presented at the Communication OC213 at Euromembrane 2009, held in Montpellier, France 2009.
13. Belfort G. Fluid mechanics in membrane filtration: recent developments. *J Membr Sci*. 1989;40:123–147.
14. Ghidossi R, Veyret D, Moulin P. Computational fluid dynamics applied to membranes: state of the art and opportunities. *Chem Egng Process*. 2006;45:437–454.
15. Geraldes V, Semiao V, Pinho MN. Numerical modeling of mass transfer in slits with semi-permeable membrane walls. *Engng Comput*. 2000;17:192–217.
16. Pellerin E, Michelitsh E, Darcovich K, Lin S, Tam CM. Turbulent transport in membrane modules by CFD simulations in two dimensions. *J Membr Sci*. 1995;100:139–153.
17. Serra CA, Wiesner MR. A comparison of rotating and stationary membrane disk filters using computational fluid dynamics. *J Membr Sci*. 2000;165:19–29.
18. Bellhouse BJ, Costigan G, Abhinava K, Merry A. The performance of helical screw-thread inserts in tubular membranes. *Sep Pur Technol*. 2001;22:89–113.
19. Kieffer R, Charcosset C, Puel F, Mangin D. Numerical mass transfer in a liquid-liquid membrane contactor for laminar flow conditions. *Comp Chem Engng*. 2008;32:1325–1333.
20. deMontigny D, Tontiwashwuthikul P, Shakma A. Using polypropylene and polytetrafluoroethylene membranes in a membrane contactor for CO_2 absorption. *J Membr Sci*. 2006;277:99–107.
21. Zhang HY, Wang R, Liang JH. Modeling and experimental study of CO_2 absorption in a hollow fiber membrane contactor. *J Membr Sci*. 2006;279:301–310.
22. Keshavarz P, Fathikalakahi J, Ayatollahi S. Analysis of CO_2 separation and simulation of a partially wetted hollow fiber membrane contactor. *J Hazard Mater*. 2008;152:1237–1247.
23. Gong Y, Wang Z, Wang S. Experiments and simulation of CO_2 removal by mixed amines in a hollow fiber membrane module. *Chem Eng Process*. 2006;45:652–660.
24. Shirazian S, Ashrafizadeh SN. Mass transfer simulation of carbon dioxide absorption in a hollow fiber membrane contactor. *Sep Sci Tech*. 2010;45:515–524.
25. Danckwerts PV. The reactions of CO_2 with ethanolamines. *Chem Eng Sci*. 1979;34:443–446.
26. Hikita H, Asai S, Ishikawa H, Honda M. The kinetics of reactions of carbon dioxide with diethanolamine and triethanolamine by a rapid mixing method. *Chem Eng J*. 1977;13:7–12.
27. Bird RB, Stewart WE, Lightfoot EN. *Transport Phenomena*. New York: Wiley, 1960.
28. Skelland AHP. *Diffusional Mass Transfer*. New York: Wiley, 1974.
29. Treybal RE. *Mass-Transfer Operations*, 3rd ed. New York: McGraw-Hill, 1987.
30. Prasad R, Sirkar KK. Dispersion-free solvent extraction with microporous hollow fiber membrane. *AIChE J*. 1988;34:177–188.
31. Yang MC, Cussler EL. Designing hollow fiber contactors. *AIChE J*. 1986;32:1910–1916.
32. Cussler EL. *Diffusion Mass Transfer in Fluid Systems*. Cambridge: Cambridge University Press, 1984.
33. deCoursey WJ. Enhancement factor for gas absorption with reversible chemical reaction. *Chem Eng Sci*. 1982;37:1483–1489.
34. Zimmerman WBJ. *Process Modeling and Simulation with Finite Elements*. New Jersey: World Scientific, 2004.

35. Finlayson BA. *Introduction to Chemical Engineering Computing*. New York: Wiley, 2006.
36. Kumar PS, Hogendoorn JA, Feron PHM, Versteeg GF. Approximate solution to predict the enhancement factor for the reactive absorption of a gas in a liquid flowing through a microscopic membrane hollow fiber. *J Membr Sci*. 2003;213:231–245.
37. Nguyen PT. Etude de la capture du CO_2 par des contacteurs membranaires innovants. Ph.D. thesis, INPL, Nancy Université, France. 2011.
38. Versteeg GF, van Swaaij WPM. Solubility and diffusivity of acid gases CO_2, N_2O in aqueous alkanolamine solutions. *J Chem Eng Data*. 1987;33:29–34.
39. Robb WL. Thin silicone membranes: their permeation properties and some applications. *Ann NY Acad Sci*. 1968;146:119–137.
40. Snijder ED, te Riele MJM, Versteeg GF, van Swaaij WPM. Diffusion coefficients of several aqueous alkanolamine solutions. *J Chem Eng Data*. 1993;38:475–480.
41. Reid RC, Prauznitz JM, Sherwood TK. *The Properties of Gases and Liquids*, 3rd ed. New York: McGraw-Hill. 1977.

Appendix: Dimensionless Form of the Modeling Equations

Introducing the new independent and dependent variables

$$\zeta = \frac{z}{l}, \quad \xi = \frac{r}{r_e}, \quad \Phi_{Af} = \frac{[CO_2]_f}{[CO_2]_{in}}, \quad \Phi_{Bf} = \frac{[Am]_f}{C_T}$$
$$\Phi_{Am} = \frac{[CO_2]_m}{[CO_2]_{in}}, \quad \Phi_{As} = \frac{[CO_2]_s}{[CO_2]_{in}}, \quad u_{rs} = \frac{v_{rs}}{v_{zs}^0}$$
$$u_{zs} = \frac{v_{zs}}{v_{zs}^0}, \quad P = \frac{p}{\rho {v_{zs}^0}^2}$$

The mass transport governing equations in the three domains along with their corresponding boundary conditions are rewritten in a dimensionless form.

Fiber bore domain

$$\frac{(1-\xi^2)Gr_{Af}}{2}\frac{\partial \Phi_{Af}}{\partial \zeta} = \frac{1}{\xi}\frac{\partial}{\partial \xi}\left[\xi \frac{\partial \Phi_{Af}}{\partial \xi}\right] - \frac{\beta_1 Gr_{Af}\Omega_{CO_2}}{4} \quad (A1)$$

$$\frac{(1-\xi^2)Gr_{Bf}}{2}\frac{\partial \Phi_{Bf}}{\partial \zeta} = \frac{1}{\xi}\frac{\partial}{\partial \xi}\left[\xi \frac{\partial \Phi_{Bf}}{\partial \xi}\right] - \frac{\beta_1 Gr_{Bf}\Omega_{CO_2}}{2} \quad (A2)$$

where the dimensionless reaction rate is expressed as

$$\Omega_{CO_2} = \Phi_{Af}\Phi_{Bf} - \frac{\left[1-\Phi_{Bf}\right]^2}{\beta_3 \Phi_{Bf}} \quad (A3)$$

subject to the normalized boundary conditions

$$\text{at } \zeta = 0, \qquad \Phi_{Af} = 0, \qquad \Phi_{Bf} = 1, \quad \forall\, 1 \geq \xi \geq 0 \quad (A4)$$

$$\text{at } \xi = 0, \qquad \frac{\partial \Phi_{Af}}{\partial \xi} = 0, \qquad \frac{\partial \Phi_{Bf}}{\partial \xi} = 0, \quad \forall\, 1 \geq \zeta \geq 0 \quad (A5)$$

$$\text{at } \xi = \lambda_1 = \frac{r_i}{r_e}, \quad \frac{\partial \Phi_{Af}}{\partial \xi} = \left[\Phi_{Am} - \frac{\Phi_{Af}}{\mathcal{H}_{CO_2}}\right]\frac{\alpha_1}{\lambda_1\left(\ln \xi - \ln \lambda_1\right)}$$
$$\frac{\partial \Phi_{Bf}}{\partial \xi} = 0, \quad \forall\, 1 \geq \zeta \geq 0 \quad (A6)$$

The third boundary condition is obtained by solving the transport equation through the membrane material for the first flux continuity. The same procedure is applied to the second boundary condition to which the shell mass transport is constrained.

Polymeric membrane domain

$$\frac{1}{\xi}\frac{\partial}{\partial \xi}\left[\xi \frac{\partial \Phi_{Am}}{\partial \xi}\right] = 0 \quad (A7)$$

subject to the normalized boundary conditions

$$\text{at } \xi = \lambda_1 = \frac{r_i}{r_e}, \qquad \Phi_{Am} = \frac{\Phi_{Af}}{\mathcal{H}_{CO_2}} \qquad \forall\, 1 \geq \zeta \geq 0 \quad (A8)$$

$$\text{at } \xi = \lambda_2 = \frac{r_o}{r_e}, \qquad \Phi_{Am} = \Phi_{As} \qquad \forall\, 1 \geq \zeta \geq 0 \quad (A9)$$

Shell domain

- Plug flow

$$\frac{d\phi_{As}}{d\zeta} = Da_{ext}\left[\phi_{As} - \frac{\phi_{Af}}{m}\right] \quad (A10)$$

where $Da_{ext} = \frac{4nd_o k_{CO_2 s} l}{v_{zs}^0 d_s^2 (1-\varphi)}$.

- Happel flow

$$v_{zs} = 2v_{zs}^0 \varepsilon \left\{ \frac{\varepsilon - 1 + (1-\varepsilon)\left(\frac{r}{r_o}\right)^2 - \ln\left(\frac{r}{r_o}\right)^2}{\varepsilon(\varepsilon+2) + \ln(1-\varepsilon)^2} \right\} \quad (A11)$$

- Navier-Stokes flow

$$\frac{u_{zs}Gr_{As}}{4}\frac{\partial \Phi_{As}}{\partial \zeta} = \frac{1}{\xi}\frac{\partial}{\partial \xi}\left[\xi \frac{\partial \Phi_{As}}{\partial \xi}\right] \quad (A12)$$

$$\frac{1}{\xi}\frac{\partial}{\partial \xi}(\xi u_{rs}) + \frac{\partial u_{zs}}{\partial \zeta} = 0 \quad (A13)$$

$$u_{rs}\frac{\partial u_{rs}}{\partial \xi} + u_{zs}\frac{\partial u_{rs}}{\partial \zeta} = \frac{1}{Re_{As}}\left[\frac{\partial}{\partial \xi}\left(\frac{1}{\xi}\frac{\partial}{\partial \xi}(\xi u_{rs})\right) + \frac{\partial^2 u_{rs}}{\partial \zeta^2}\right] \quad (A14)$$

$$u_{rs}\frac{\partial u_{zs}}{\partial \xi} + u_{zs}\frac{\partial u_{zs}}{\partial \zeta} = -\frac{\partial P}{\partial \zeta} + \frac{1}{Re_{As}}\left[\frac{1}{\xi}\frac{\partial}{\partial \xi}\left(\xi \frac{\partial u_{zs}}{\partial \xi}\right) + \frac{\partial^2 u_{zs}}{\partial \zeta^2}\right] \quad (A15)$$

subject to the normalized boundary conditions

$$\text{at } \zeta = 0, \qquad P = 1 \qquad \forall\, 1 \geq \xi \geq 0 \quad (A16)$$

$$\text{at } \xi = \lambda_2 = \frac{r_o}{r_e}, \quad \frac{\partial \Phi_{As}}{\partial \xi} = \left[\Phi_{Am} - \frac{\Phi_{As}}{\mathcal{H}_{CO_2}}\right]\frac{\alpha_2}{\lambda_2\left(\ln \xi - \ln \lambda_2\right)},$$
$$u_{rs} = 0, \qquad u_{zs} = 0, \quad \forall\, 1 \geq \zeta \geq 0 \quad (A17)$$

$$\text{at } \xi = 1, \quad \frac{\partial \Phi_{As}}{\partial \xi} = 0, \qquad u_{rs} = 0, \qquad u_{zs} = 1, \qquad \forall\, 1 \geq \zeta \geq 0 \tag{A18}$$

$$\text{at } \zeta = 1, \qquad \Phi_{As} = 1, \quad u_{rs} = 0, \qquad u_{zs} = 0, \quad \forall\, 1 \geq \xi \geq 0 \tag{A19}$$

Note that all three dimensionless Graetz numbers are based on the equivalent fiber diameter d_e. The outlet mixing cup concentration rewritten in a dimensionless form is

$$\Phi_{Afo} = 4 \int_0^{\lambda_1} \xi(1 - \xi^2)\Phi_{Af} d\xi \tag{A20}$$

$$\Phi_{Aso} = \frac{\int_{\lambda_2}^1 \xi u_{zs} \Phi_{As} d\xi}{\int_{\lambda_2}^1 \xi u_{zs} d\xi} \tag{A21}$$

The extent of the soluble gas removal Ψ which expresses the percentage of the recovered solute is defined in the fiber bore as

$$\Psi_{Afo} = \frac{[CO_2]_f^{in} - [CO_2]_f^{out}}{[CO_2]_f^{in}} = 1 - \Phi_{Afo} \tag{A22}$$

and, similarly for the solute in the gas stream

$$\Psi_{Aso} = \frac{[CO_2]_s^{in} - [CO_2]_s^{out}}{[CO_2]_s^{in}} = 1 - \Phi_{Aso} \tag{A23}$$

Because the CO_2 concentration range studied is too small, the change between volumetric feed and exit gas streams is negligible. For that, the CO_2 absorption flux is estimated by making a mass balance over the reactor

$$\mathcal{J}_{CO_2} = \frac{V[CO_2]_{in}(1 - \Phi_{Aso})}{n\pi d_i l} \tag{A24}$$

Table A1. Dimensionless Groupings Definition

Designation	Symbol	Expression
Graetz number of CO_2 in fiber side	Gr_{Af}	$\frac{v_{zf}^0 d_e^2}{l\mathcal{D}_{CO_2 f}}$
Graetz number of MEA in fiber side	Gr_{Bf}	$\frac{v_{zf}^0 d_e^2}{l\mathcal{D}_{Amf}}$
Graetz number of CO_2 in shell side	Gr_{As}	$\frac{v_{zs}^0 d_e^2}{l\mathcal{D}_{CO_2 s}}$
Reynolds number of CO_2 in shell side	Re_{As}	$\frac{v_{zs}^0 d_s^2}{4\eta_{CO_2} l}$
Reaction parameter of MEA in the fiber	β_1	$\frac{k_1 l C_T}{v_{zf}^0}$
Reaction parameter of CO_2 in the fiber	β_2	$\frac{k_1 l [CO_2]_{in}}{v_{zf}^0}$
Reaction parameter relative to the equilibrium	β_3	$4K_{eq}[CO_2]_{in}$
First diffusivity ratio	α_1	$\frac{\mathcal{D}_{CO_2 m}}{\mathcal{D}_{CO_2 f}}$
Second diffusivity ratio	α_2	$\frac{\mathcal{D}_{CO_2 m}}{\mathcal{D}_{CO_2 s}}$

The introduction of the above new variables gives birth to the new dimensionless groupings summarized and listed in Table A1.

Manuscript received Oct. 26, 2010, revision received Aug. 18, 2011, and final revision received Oct. 5, 2011.